

---

# OpticalRS-4M: Scaling Efficient Masked Autoencoder Learning on Large Remote Sensing Dataset

---

Fengxiang Wang<sup>1</sup>, Hongzhen Wang<sup>2\*</sup>, Di Wang<sup>3</sup>, Zonghao Guo<sup>4</sup>, Zhenyu Zhong<sup>5</sup>,  
Long Lan<sup>1\*</sup>, Jing Zhang<sup>6\*</sup>, Zhiyuan Liu<sup>2</sup>, Maosong Sun<sup>2</sup>

<sup>1</sup> National University of Defense Technology, China <sup>2</sup> Tsinghua University, China

<sup>3</sup> Wuhan University, China <sup>4</sup> University of Chinese Academic of Sciences, China

<sup>5</sup> Nankai University, China <sup>6</sup> The University of Sydney, Australia

## Abstract

Masked Image Modeling (MIM) has become an essential method for building foundational visual models in remote sensing (RS). However, the limitations in size and diversity of existing RS datasets restrict the ability of MIM methods to learn generalizable representations. **Additionally, conventional MIM techniques, which require reconstructing all tokens, introduce unnecessary computational overhead.** To address these issues, we present a new pre-training pipeline for RS models, featuring the creation of a large-scale RS dataset and an efficient MIM approach. We curated a high-quality dataset named **OpticalRS-4M** by collecting publicly available RS datasets and processing them through exclusion, slicing, and deduplication. OpticalRS-4M comprises 4 million optical images covering various RS tasks, such as object detection and pixel segmentation. To enhance efficiency, we propose SelectiveMAE, a pre-training method that dynamically encodes and reconstructs semantically rich patch tokens, thereby reducing the inefficiencies of traditional MIM models caused by redundant background pixels in RS images. Extensive experiments demonstrate that OpticalRS-4M significantly improves classification, detection, and segmentation performance, while SelectiveMAE increases training efficiency over  $2\times$  times. This highlights the effectiveness and scalability of our pipeline in developing RS foundational models. The dataset, source code, and trained models will be released at [OpticalRS-4M](#).

## 1 Introduction

Over the past decade, advancements in remote sensing (RS) technology and data acquisition have improved applications in ecosystem monitoring [1], natural disaster management [2], among others [3, 4]. These applications rely on essential capabilities such as scene classification [5, 6], object detection [7], change detection [8], and semantic segmentation [9]. However, each of these downstream tasks often requires substantial computational resources to learn task-specific feature representations and develop specialized models.

Thanks to advances in self-supervised learning methods, such as Masked Image Modeling (MIM) techniques [10, 11], the pre-training of visual foundation models has seen remarkable improvements [12–17]. Consequently, remote sensing foundation models (RSFMs) have recently emerged, offering general feature representations and achieving outstanding performance across various remote sensing downstream tasks [18]. However, two challenges persist in the development of RSFMs. (i) Compared to the ImageNet-21k [19] dataset, previous RS datasets [20–23] contain fewer samples (approximately 1 million vs. 14 million), which impedes the sufficient MIM training of large backbones.

---

\*Corresponding authors

(ii) These datasets, which primarily focus on global scene semantics [20–22], lack the diversity and fine-grained information of RS scenarios encountered in downstream tasks. This limitation restricts the generalization of the learned representations.

To address these challenges, we propose a new pipeline to collect, create, and efficiently process a large optical RS dataset. Firstly, we reviewed publicly available remote sensing datasets from the past decade and selected them based on the DiRS (Diversity, Richness, and Scalability) principle [20]. Nevertheless, issues such as inconsistent data sources, excessively large image sizes, and redundant pixels still exist. Therefore, we also apply exclusion, slicing, and deduplication processes to further improve data quality. Correspondingly, we obtain a large-scale RS dataset called **OpticalRS-4M** comprising 4 million optical images, which is designed to fully leverage the representation learning capabilities of MIM methods in RS applications. OpticalRS-4M exceeds previous RS datasets [24, 21, 25–36, 18, 37, 38], being at least four times larger. Moreover, OpticalRS-4M encompasses a wide range of diverse RS scenarios encountered in downstream tasks such as object-level detection and pixel-level segmentation (Fig. 1 left).

Despite substantial efforts in training RSFM using MIM methods, such as leveraging general image knowledge [25, 26, 28], expanding parameter scales [29], integrating spatio-temporal information [30–32], and learning multi-scale features [33, 35, 36], the computational burden and slow convergence when employing MIM training on large-scale RS datasets cannot be ignored. Specifically, pre-training on 1 million RS samples requires 107 hours for the ViT-B [39] backbone on 8 Nvidia A100 GPUs [18]. **This issue becomes even more pronounced when training on larger datasets, e.g., OpticalRS-4M.** In natural scene analysis, this issue has led to numerous studies [40–45] aimed at improving MIM training efficiency. One approach is to accelerate the token reconstruction process by using decoders with fewer parameters [40, 41]. Another approach is to reduce the number of visible patch tokens input into the vision encoder [42–44], speeding up feature extraction.

However, conventional MIM approaches, such as the encoding-then-decoding procedure, overlook the unique characteristics of RS images, which typically feature sparse foreground pixels and dense backgrounds [18, 28]. This raises two key questions about how to efficiently conduct MIM training in the RS field: 1) Is it necessary to reconstruct all the redundant background patches during the MIM decoding process? 2) Is there a feasible way to encode fewer image patches (e.g.,  $\leq 25\%$ ) to accelerate the convergence of MIM training? To address the first question, a measure-based selection process is needed to identify the appropriate patches for reconstruction. For the second question, the intuition is that the patch tokens used in the encoding-then-decoding procedure should effectively capture feature dependencies in RS images.

Regarding the above issues, in the second part of the pipeline, we introduce a MIM method called **SelectiveMAE for efficiently processing RS images, which dynamically encodes and reconstructs patch tokens based on their semantic richness.** Specifically, SelectiveMAE utilizes the Histogram of Oriented Gradients (HOG) algorithm to quantify the semantic richness of patches. Then, it selects a subset of patch tokens (e.g.,  $\leq 50\%$ ) with higher HOG values for feature encoding (e.g.,  $\leq 15\%$ ) and pixel reconstruction (e.g.,  $\leq 35\%$ ). However, using an extremely low ratio of visible patches during MIM training can lead to gradient explosion or vanishing. To mitigate this, we designed a Progressive Semantic Token Selection (PSTS) module, which dynamically selects semantically relevant patch tokens during the entire training phase. In the beginning, SelectiveMAE encodes semantically rich tokens and reconstructs semantically similar ones to warm up the training process. As training advances, SelectiveMAE shifts to reconstructing high-semantic tokens from encoded lower-semantic ones to capture complementary semantic dependencies. This analogical-to-complementary strategy allows SelectiveMAE to efficiently and progressively learn robust representations of RS images while accelerating MIM convergence. Our experiments reveal that 40% of RS image patches are sufficient to train a comparable model, offering new insights into MIM training on RS images.

The contributions of this paper are summarized as follows:

- 1) We introduce a new pipeline to collect, create, and efficiently process a large optical RS dataset for developing RS foundation models.
- 2) Using this pipeline, we create the OpticalRS-4M dataset, which is a large-scale RS dataset comprising 4 million optical images with diversified coverage scenarios.

3) We introduce SelectiveMAE, an efficient MIM method tailored for RS image pre-training. It significantly accelerates convergence and enhances representation learning compared to the original MIM approach.

Experiment results suggest the effectiveness and scalability of the proposed pipeline. OpticalRS-4M significantly enhances the performance of RS foundation models in downstream tasks, while SelectiveMAE achieves over  $2\times$  speedup in pre-training compared to MAE [10].

## 2 Related Work

**Remote Sensing Datasets.** In recent years, many RS datasets have been created for tasks such as scene classification [23, 46], object detection [47–49], and segmentation [50–52]. The availability of free, unlabeled satellite images has led to the development of large-scale RS datasets. Some works combine various sensor data to create extensive datasets. SEN12MS [53] with 180,662 triplets of dual-pol synthetic aperture radar (SAR) and multi-spectral Sentinel-2 image patches. SSL4EO-S12 [54] dataset uses publicly available SAR/optical satellite data collected by the European Space Agency’s Sentinel mission. SSL4EO-L [55] consists entirely of multispectral data. SatlasPretrain [56] is constructed from data sources such as Sentinel-2, Sentinel-1, Landsat 8/9, and 0.5 - 2 meter/pixel aerial imagery. While it includes millions of images, the majority are multispectral and SAR, with only a small fraction being RGB. There are also some large-scale RS visual-language datasets such as Skyscript [57] and RS5M [58], but they primarily focus on multimodal tasks. Currently, some datasets focus solely on optical RS images. MillionAID [20] offers a million-scale dataset for RS optical image classification, while SeCo [22] and CACo [21] provide nearly a million images of the same location over different times. However, these datasets primarily target scene classification and often overlook fine-grained target information, limiting their utility for various downstream tasks. To address this gap, with the proposed pipeline, we introduce the OpticalRS-4M dataset, which is larger and more diverse, enhancing performance across multiple downstream tasks.

**Masked Image Modeling.** Inspired by the success of Masked Language Modeling (MLM) in NLP [59], MIM has been developed for visual pre-training [60, 11, 10, 61, 62]. MIM learns image representations by reconstructing masked tokens, focusing on various regression targets [63–67], masking strategies [68, 69], and reconstruction methods [70–73]. For instance, MAE [10] demonstrates that predicting pixel values can be as effective as using complex targets. A major challenge for MIM is its high computational demand and lengthy pre-training times. To mitigate this, some studies use asymmetric encoder-decoder strategies [40, 41], reduce input patches [42, 44] or use a novel Difficulty-Flatten Loss [43]. Additionally, CrossMAE [45] employs cross-attention between masked and visible tokens to enhance efficiency without sacrificing performance. However, these methods do not account for the unique characteristics of RS images, such as sparse foreground information and complex backgrounds. Considering these issues, we introduce an efficient MIM method named SelectiveMAE that significantly speeds up pre-training, enhancing the practicality of developing RS foundation models based on large-scale datasets.

**Remote Sensing Foundation Models.** Despite the abundance of RS data, much of it remains unlabeled and thus inaccessible for supervised learning [74]. Self-supervised learning methods have recently been employed to extract representations from unlabeled RS data. Although there are some contrastive self-supervised methods [24, 21, 22, 75], recent advancements have primarily centered around generative self-supervised methods. For example, RVSA [18] leverages the vision transformer backbone pre-trained by the vanilla MAE [10] method and introduces computationally efficient rotated varied-size window attention to replace the original attention during fine-tuning. In addition, many studies are focusing on improving generative self-supervised algorithms by leveraging general image knowledge [25, 26, 28], scaling up parameter sizes [29], integrating spatio-temporal data [30–32], handling multi-sensor data [76–80], and employing multi-scale concepts [33, 35, 36]. However, these methods have not effectively addressed the substantial computational burden associated with self-supervised pre-training in RS. In the paper, we propose a new pipeline that can collect, create, and efficiently process large amounts of optical RS data for developing RS foundation models, enhancing the practicality of MIM pre-training on large-scale datasets.

### 3 Methodology

The proposed pipeline contains two critical components: dataset generation and efficient pre-training, which will be introduced in detail in the following text.

#### 3.1 Dataset Generation

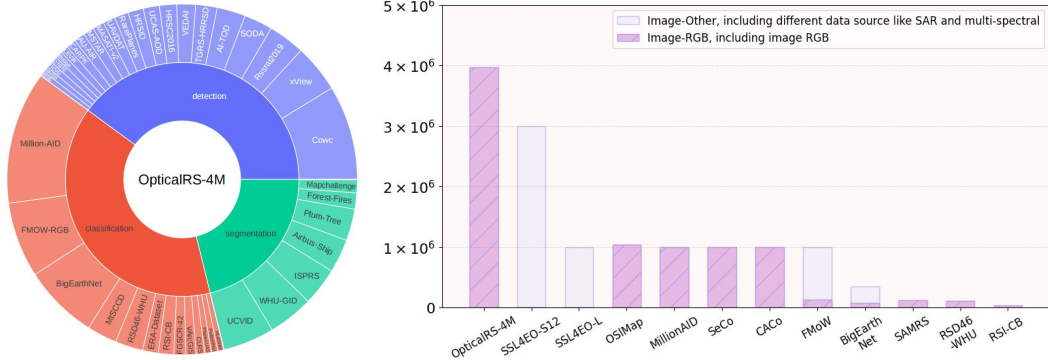


Figure 1: **Left:** The organization of data sources in OpticalRS-4M. **Right:** The comparison between OpticalRS-4M and other datasets.

Recent progress in self-supervised pre-training for RSFMs is limited by the relatively small scale and diversity of existing RS datasets compared to natural scene datasets. To overcome this, we first curate a large-scale RS dataset, OpticalRS-4M, through extensive data collection and preprocessing.

##### 3.1.1 Data Collection

We began by reviewing publicly available RS datasets from the past decade. Recognizing that not all data are suitable for self-supervised pre-training, we adopted specific criteria for data collection, as outlined in DiRS [20]: **1) Diversity:** A dataset is diverse if its images capture various typical visual features of relevant scenes or targets and offer complementarity. **Intra-class Diversity:** High diversity within classes ensures comprehensive representation of real-world target distributions. To ensure this, we consider the data from different sources of the same scene or target. Moreover, in the RS field, the attributes of objects may vary with geographic location and imaging time, so the change detection data is also incorporated. **Inter-class Diversity:** To enable self-supervised pre-training to distinguish between categories effectively, we incorporated as many fine-grained categories as possible, especially those with high semantic overlap. This strategy helps the model learn robust feature representations. **2) Richness:** Beyond diversity, richness is also essential. We ensure diverse content features and large sample sizes by collecting images under various conditions — weather, seasons, lighting, and so on — introducing variability in translation, viewpoint, object posture, spatial resolution, background, and occlusion. Our data collection process actively includes the sample of the same category under different imaging conditions to ensure comprehensive real-world representation, enhancing the model’s representation and generalization capabilities. **3) Scalability:** Given the evolving applications of remote sensing images, scalability is also crucial. We constantly enrich the dataset based on scene and target categories across classification, detection, and segmentation tasks.

In summary, following the guidelines, we constructed a large-scale RS image dataset with diverse coverage scenarios. Fig. 1 left illustrates the included RS datasets collected.

##### 3.1.2 Data Preprocessing

Following data collection, challenges such as inconsistent data sources, oversized images, and redundant pixels remained. To address these, we implemented a standardized, scalable data preprocessing workflow consisting of four steps:

- 1) We focused exclusively on optical images for this study, excluding multispectral and SAR data, though future updates will incorporate these modalities for multi-modal self-supervised pre-training.
- 2) To manage the large image sizes, we randomly cropped high-resolution images into smaller slices.

3) We filtered out images with fewer than 64 or more than 1024 pixels. 4) The remaining images were combined and duplicates were removed using a two-phase approach: first, a coarse phase with perceptual hashing [81], and then a refined phase involving manual review. This ensured that only highly similar images were excluded. As a result of these steps, we created the OpticalRS-4M dataset, which contains approximately 4 million high-quality RS images — significantly larger than previous representative RS datasets, as illustrated in Fig. 1 right.

In summary, we followed the DiRS principles for data collection, applying exclusion, slicing, and deduplication to ensure high-quality results. We’ve screened and processed most small and medium-scale datasets from the past decade in this field. More efforts can be made to extend OpticalRS-4M by including larger datasets like SSL4EO-S12 [54] and SSL4EO-L [55] to enhance dataset capacity.

### 3.1.3 Dataset Diversity

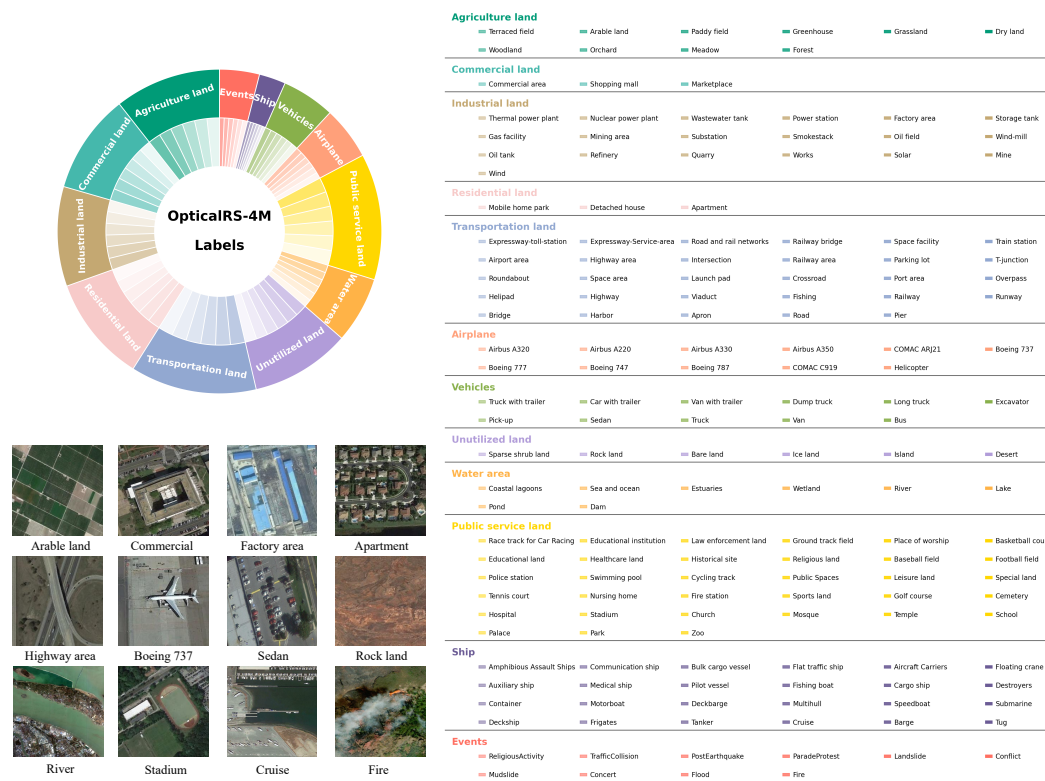


Figure 2: **Left:** Main categories with visual examples from OpticalRS-4M. **Right:** Full hierarchy of OpticalRS-4M categories.

To demonstrate the broad scope of scenes and target categories covered by our dataset, we conducted a statistical analysis accompanied by a detailed label explanation, reviewing all the scenarios and targets included in OpticalRS-4M, as shown in Fig. 2. The analysis reveals that OpticalRS-4M comprises 12 main categories, each containing numerous subclasses. Unlike existing self-supervised optical remote sensing datasets, OpticalRS-4M not only offers more comprehensive scene and target information but also introduces “Events” as a distinct high-level category. This category includes labels such as “Concert”, “Parade/Protest”, “Religious Activity”, “Fire”, “Flood”, “Landslide”, “Post-Earthquake”, and “Traffic Collision”. This expanded information enhances the versatility of OpticalRS-4M for a wider range of downstream tasks.

### 3.2 Efficient Pre-training

After obtaining a large-scale RS dataset, the next step is to conduct the self-supervised pre-training. However, as the capacity of the dataset grows, vast computational and time costs are required for existing MIM approaches used in the RS community, *e.g.*, MAE [10]. To address this issue, our pipeline introduces an efficient MIM method, *i.e.*, SelectiveMAE. In this section, we first review the preliminaries of MAE, then we present the details of SelectiveMAE.

#### 3.2.1 Masked Autoencoders Preliminaries

**1) Masking.** Similar to supervised training of a standard ViT, MAE divides the image into regular, non-overlapping patches. It then samples a subset of these patches and masks the remaining ones. Typically, the masking ratio is 75%, meaning only 25% of the patches are input to the encoder. This random sampling follows a uniform distribution according to the masking ratio. **2) MAE Encoder.** The encoder is a standard ViT applied only to the visible, unmasked patches. It linearly projects the patches, adds positional embeddings, and processes them through a series of transformer blocks. By operating on a smaller subset of patches, the encoder enables the training of large models with reduced computational and memory requirements. **3) MAE Decoder.** The encoded tokens and masked tokens are fed into the decoder, which comprises transformer blocks with self-attention layers. The masked tokens are shared, learnable tensors enhanced with positional embeddings. The decoder, utilized only during pre-training, generates the output predictions for those masked tokens. **4) Reconstruction Target.** MAE predicts the pixel values for each masked patch, with each element in the decoder output representing a patch’s pixel value vector. The loss function computes the mean squared error (MSE) between the reconstructed targets and original patches.

RS optical images typically contain many redundant background pixels, which aligns well with MAE’s masking strategy. In MAE, the encoder processes only 25% of the patches, reducing computational load by avoiding processing the entire image. Building on MAE, we aim to leverage the redundancy in RS images to accelerate training. Specifically, we address two questions: *1) Is it necessary to reconstruct all the masked patches given the redundancy in RS images? 2) Can the visible patches input to the MAE encoder be further compressed to enhance acceleration?*

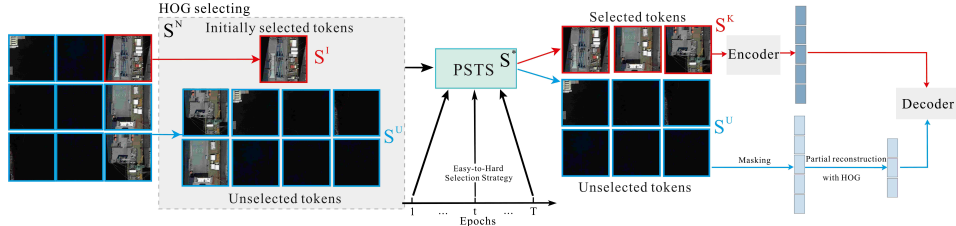


Figure 3: **Overview of SelectiveMAE.** The vanilla version of SelectiveMAE.

#### 3.2.2 Partial Reconstruction

For question 1, previous research [45] has shown that for general images, when MAE reconstructs 75% of the patches to calculate the loss, a specially designed decoder doesn’t need to fully reconstruct all remaining patches. In fact, reconstructing just 50% or even 25% of the patches can achieve similar performance and speed up training. However, for RS images, if we randomly sample patches and remove most for reconstruction, the reconstructed patches might not be semantically rich ones. Using only a random subset for reconstruction even degrades performance.

To address this issue, we propose selecting semantically rich patches for reconstruction instead of random selection. Specifically, given an input image  $x \in \mathbb{R}^{H \times W \times C}$ , it is reshaped into  $N = (H \times W)/p^2$  non-overlapping patches  $x^p \in \mathbb{R}^{N \times (p^2 C)}$ , where  $p$  is the patch size,  $(H, W)$  is the size of the input image, and  $C$  is the number of channels. These patches  $\{x_i^p\}_{i=1}^N$  are then linearly mapped to patch embeddings. To retain positional information, positional embeddings are added to the patches. We select a portion of the patches to input to the encoder based on the masking ratio  $m \in [0, 1]$  ( $m = 85\%$  by default), as detailed in Sec. 3.2.1. The remaining patches serve as reconstruction targets for the decoder. Unlike MAE’s masking ratio, we introduce a new reconstruction ratio  $r$ , the proportion of pixels to be reconstructed, denoted as  $r \in [0, m]$  ( $r = 25\%$  by default). We compute

the HOG features  $HOG(\cdot)$  of the remaining patches and select those with the high HOG feature values according to the reconstruction ratio  $r$ , rather than using all patches. The process can be formulated as:

$$token_R = \{x_i^p | i \in top_{\lfloor r \times N \rfloor}(HOG(\{x_i^p\}_{i=1}^{m \times N}))\}, \quad (1)$$

where  $token_R$  denotes the selected mask tokens for reconstruction and  $top_n(\cdot)$  denotes the index set of the selected top  $n$  tokens. The decoder uses a lightweight design based on cross-attention following CrossMAE [45]. **Experimental results in the Appendix show that this partial reconstruction strategy significantly increases the training throughput without affecting the learned representations.**

### 3.2.3 Progressive Semantic Token Selection

For the second question, we initially tried a naive approach by increasing the masking ratio to 85%, meaning only 15% of the patches in each RS image were input to the encoder while keeping a 25% reconstruction ratio as proposed in Sec. 3.2.2. However, during training, this setup often led to issues like gradient explosions or loss divergence (see the Appendix). We speculate that, although RS images have background redundancy, using such a small portion of patches challenges MAE training. How can we achieve acceleration at a high masking ratio while ensuring MAE convergence? Curriculum learning [82–84] may offer a solution. However, it typically focuses on selecting whole image samples, whereas MIM pre-training masks large portions of image pixels, emphasizing patch-level selection. Therefore, it’s essential to distinguish between “easy” and “hard” patches in MIM pre-training.

To this end, we introduce the Progressive Semantic Token Selection (PSTS) module for patch selection. In this module, depicted in Fig. 3, we begin by selecting a limited number of patches and then select additional patches based on them in the training epoch, dynamically transitioning from easily learned, semantically similar patches to more challenging, complementary ones.

For initialization, we employ a HOG selection strategy to choose the initial patch set. This simple yet effective strategy ensures that semantically rich tokens are selected. Following token initialization, we aim to incrementally increase the number of tokens to facilitate a training progression from easy to difficult, while adhering to the final masking ratio for selected tokens. This process is outlined in the Appendix. Given the initial token sets’ high HOG feature values, nearby tokens selected by PSTS also exhibit high HOG feature values. Recalling our partial reconstruction approach in Sec. 3.2.2, we filter the remaining unselected token set to include those with high HOG values as reconstruction targets. Consequently, when selecting nearby tokens, the tokens input for encoding and those chosen for reconstruction are closer, thereby simplifying the training process. Conversely, if a token’s feature distribution deviates from others in the set, indicating it is farther away, we consider such patches more challenging to learn. **Details of the process are presented in the Appendix.**

## 4 Experiment

**In this section, we first discuss the effectiveness of the dataset and acceleration strategy in the pipeline through ablation experiments. We also conducted further experiments to test the scalability of the pipeline in the ablation experiments. Additionally, we performed comprehensive comparative experiments to evaluate the pipeline’s performance on downstream tasks.**

**Pre-training Setup.** Our pre-training experiment setup largely follows MAE [10]. The masking ratio is 85%, and the reconstruction ratio is 25%. For patch selection, the adjustment threshold is set at 300 epochs, with the last 200 epochs using random distance to enhance robustness.

### 4.1 Ablation Study

**To validate the pipeline’s effectiveness, we conducted separate evaluations of both the OpticalRS-4M dataset generated by the pipeline and the accelerated training method, SelectiveMAE. Additionally, we assessed the pipeline’s scalability in collecting and processing datasets of varying sizes.**

#### 4.1.1 Superiority of OpticalRS-4M

**Dataset Diversity.** In self-supervised pre-training of RSFMs, the primary goal is to enhance downstream task performance. We define dataset diversity as its ability to improve various types of these

Table 1: Comparison of downstream task performance at matched data throughput between MillionAID and OpticalRS-4M, assessed using MAE [10] pre-training and ViT Base models [39].

Dataset	Method	Images Number	Epoch	Sense Classification		Object Detection		Semantic Segmentation	
				AID	RESISC-45	DIOR	DIOR-R	LoveDA	SpaceNetv1
				OA (TR=20% / 50%)	OA (TR=10% / 20%)	mAP <sub>50</sub>	mAP <sub>50</sub>	mIoU	mF1
MillionAID	MAE	1 million	800	94.92/97.38	89.20/93.60	71.80	62.33	51.24	79.24
OpticalRS-4M	MAE	1 million	800	96.26/97.98	91.53/93.88	<b>75.90</b>	66.46	<b>53.10</b>	79.35
OpticalRS-4M	MAE	2 million	400	96.64/98.10	91.80/94.31	73.90	65.95	52.86	79.37
OpticalRS-4M	MAE	3 million	267	<b>96.67/98.18</b>	92.24/ <b>94.41</b>	75.40	<b>67.07</b>	52.39	<b>79.37</b>
OpticalRS-4M	MAE	4 million	200	96.10/98.03	<b>92.38/94.30</b>	74.70	66.26	52.75	79.23

tasks. While datasets like MillionAID focus on classification, our OpticalRS-4M dataset is designed to extend the benefit to detection and segmentation tasks. We assess this by evaluating the effectiveness of models trained on different datasets with equivalent data throughput. For instance, MillionAID, with 1 million samples, is trained using the basic MAE method for 800 epochs as a benchmark. To showcase the diversity of OpticalRS-4M, containing 4 million samples, we train it with MAE for just 200 epochs. Additionally, we validate OpticalRS-4M’s diversity by progressively reducing its training data — down to 3 million, 2 million, or even 1 million samples — while keeping data throughput constant. As shown in Table 1, our experiments demonstrate that even when randomly sampling 1 million images from OpticalRS-4M, it outperforms MillionAID in downstream tasks, particularly in object detection and segmentation. This consistent superior performance, even with fewer images, highlights OpticalRS-4M’s greater diversity and effectiveness, emphasizing the benefits of using larger and more varied datasets for unsupervised pre-training.

The results in Table 1 indicate that the optimal outcomes at equivalent data throughput are achieved with 3 million samples rather than 4 million. In most cases, the model pre-trained on 3 million samples outperforms across various downstream tasks. Notably, on the DIOR and LoveDA datasets, the best results were obtained with 1 million samples trained for 800 epochs. However, as shown in Table 2, when we extended the training on 4 million samples to more epochs, the model achieved the highest average performance across most downstream tasks. This suggests that training on 4 million samples for only 200 epochs was insufficient for the MIM method to fully leverage the large dataset, resulting in inferior generalization in downstream tasks.

Table 2: Performance on downstream tasks with extended training on OpticalRS-4M.

Dataset	Method	Images Number	Epoch	Sense Classification		Object Detection		Semantic Segmentation	
				AID	RESISC-45	DIOR	DIOR-R	LoveDA	SpaceNetv1
				OA (TR=20% / 50%)	OA (TR=10% / 20%)	mAP <sub>50</sub>	mAP <sub>50</sub>	mIoU	mF1
OpticalRS-4M	MAE	3 million	267	96.67/98.18	92.24/94.41	75.40	67.07	52.39	79.37
OpticalRS-4M	MAE	4 million	100	95.12/97.54	91.26/93.85	-	-	-	-
OpticalRS-4M	MAE	4 million	200	96.10/98.03	92.38/94.30	74.70	66.26	52.75	79.23
OpticalRS-4M	MAE	4 million	400	96.36/98.16	92.41/94.03	-	-	-	-
OpticalRS-4M	MAE	4 million	800	<b>96.88/98.22</b>	<b>92.44/94.43</b>	<b>75.40</b>	<b>67.35</b>	<b>52.80</b>	<b>79.41</b>

**Extended training on OpticalRS-4M.** To maximize the potential of OpticalRS-4M, we extended training using the MAE pre-training method and ViT-B, varying only the number of training epochs while keeping other settings consistent. The fine-tuning results, shown in Table 2, reveal that as the number of epochs increases, OpticalRS-4M shows greater advantages in downstream tasks. This indicates that extended training is necessary to fully harness OpticalRS-4M’s capabilities. However, the gains diminish with additional epochs, suggesting that merely increasing epochs may not suffice. To unlock the full potential of OpticalRS-4M, exploring more effective pre-training methods, such as the proposed SelectiveMAE, may be crucial.

#### 4.1.2 Effectiveness of SelectiveMAE

**Performance Advantage.** To further validate the accelerated pre-training strategy of our pipeline, we conducted extensive experiments on OpticalRS-4M using both MAE [10] and SelectiveMAE. The performance of ViT-B on various downstream tasks after pre-training is presented in Table 3. The results indicate that after pre-training on OpticalRS-4M, SelectiveMAE not only outperforms MAE



Table 3: Comparison of downstream task performance using SelectiveMAE and MAE [10]. The training time is measured using 8 NVIDIA A100 GPUs.

Method	Dataset	Epoch	Total Training Hours	Scene Classification		Object Detection		Semantic Segmentation	
				AID	RESISC-45	DIOR	DIOR-R	LoveDA	SpaceNetv1
				OA (TR=20% / 50%)	OA (TR=10% / 20%)	mAP <sub>50</sub>	mAP <sub>50</sub>	mIoU	mF1
MAE	OpticalRS-4M	800	177	<b>96.88/98.22</b>	92.44/94.43	75.40	67.35	52.80	79.41
SelectiveMAE	OpticalRS-4M	800	<b>86 (2.1×)</b>	96.78/98.12	<b>93.35/94.58</b>	<b>75.70</b>	<b>67.78</b>	<b>53.05</b>	<b>79.50</b>

but also achieves this at 2.1 times the speed. This makes SelectiveMAE particularly well-suited for large-scale datasets, offering significant time savings during training on OpticalRS-4M.

Table 4: The accelerating performance of SelectiveMAE for different backbones compared to MAE [10]. The training time is measured using 8 NVIDIA A100 GPUs.

Model	Backbone	Params	Total Training Hours
MAE	ViT-B	86M	101
SelectiveMAE	ViT-B	86M	<b>48 (2.1×)</b>
MAE	ViT-L	307M	113
SelectiveMAE	ViT-L	307M	<b>50 (2.3×)</b>

**Pre-training Efficiency.** To further highlight the efficiency advantage of SelectiveMAE, we evaluate the pretraining time with different backbones on the MillionAID dataset, as shown in Table 4. It can be seen that, since only 40% of the image patches (15% for the encoder and 25% for the decoder) are involved in the calculation, our methods present more than doubled acceleration for both base and large ViT models compared to the vanilla MAE baseline, where the acceleration advantage is more significant for larger sized models.

#### 4.1.3 Scalability of the Pipeline

To evaluate the scalability of our pipeline, we organized datasets containing 1 million and 4 million samples and conducted experiments on each. The results, presented in Table 5, show that with 1 million samples, the proposed SelectiveMAE method reduced training time by 29 hours. When the dataset was expanded to 4 million samples, the time savings increased to 81 hours. These findings demonstrate that our pipeline scales effectively with larger datasets, offering significant pre-training acceleration.

Table 5: Training cost (measured using 8 NVIDIA A100 GPUs) of SelectiveMAE and MAE [10] on OpticalRS-4M with different data volumes.

Method	Images Number	Epoch	Total Training Hours
MAE	1 million	800	54
SelectiveMAE	1 million	800	<b>25 (-29)</b>
MAE	4 million	800	177
SelectiveMAE	4 million	800	<b>86 (-81)</b>

## 4.2 Main Results

### 4.2.1 Fine-tuning Performance on Downstream Tasks

We further evaluated SelectiveMAE with the OpticalRS-4M dataset across three key downstream tasks: scene classification, object detection, and semantic segmentation. In addition to benchmarking against MAE-based approaches like SatMAE[30], ScaleMAE[33], SSL4EO[54], RVSA [18], RingMo[37], and GFM[25], we compared it with other leading visual foundation models. These encompass methods leveraging contrastive learning and enhanced backbones, such as GASSL [24], SeCo [22], TOV [28], and CACo [21], and advanced supervised learning-based approaches [56]. Notably, none of these comparative methods were specifically tailored for accelerated pre-training, and although their speed performance wasn’t reported, we anticipate they may lag behind the computationally efficient baseline (MAE). More details can be found in the Appendix.

**Scene Classification.** We begin by evaluating the pre-trained model’s performance on the scene classification task, which offers insight into its overall representation capability without requiring additional decoders. We leverage two scene classification datasets: AID [85] and RESISC-45 [86]. Training details, including the training and test split ratio, adhere to [18, 33], with further specifics

Table 6: Results for scene classification, object detection, and semantic segmentation. “TR” represents the ratio of training data to the entire dataset.

Model	Publication	Backbone	Scene Classification		Object Detection		Semantic Segmentation	
			AID	RESISC-45	DIOR	DIOR-R	LoveDA	SpaceNetv1
			(TR=20%/50%)	(TR=10%/20%)	mAP <sub>50</sub>	mAP <sub>50</sub>	mIoU	mF1
SeCo [22]	ICCV’21	ResNet-50	93.47/95.99	89.64/92.91	-	-	43.63	77.09
GASSL [24]	ICCV’21	ResNet-50	93.55/95.92	90.86/93.06	67.40	65.65	48.76	78.51
TOV [28]	JSTARS’23	ResNet-50	95.16/97.09	90.97/93.79	70.16	66.33	49.70	-
CACo [21]	CVPR’23	ResNet-50	90.88/95.05	88.28/91.94	66.91	64.10	48.89	77.94
SatMAE [30]	NIPS’22	ViT-L	95.02/96.94	91.72/94.10	70.89	65.66	-	78.07
ScaleMAE [33]	ICCV’23	ViT-L	96.44/97.58	92.63/95.04	73.81	66.47	-	-
SSL4EO [54]	GRSM’23	ViT-S	91.06/94.74	87.60/91.27	64.82	61.23	-	-
RingMo [37]	TGRS’22	Swin-B	96.90/98.34	94.25/95.67	75.90	-	-	-
SatLas [56]	ICCV’23	Swin-B	94.96/97.38	92.16/94.70	74.10	67.59	-	-
GFM [25]	ICCV’23	Swin-B	95.47/97.09	92.73/94.64	72.84	67.67	-	-
RVSA [18]	TGRS’23	ViT-B+RVSA	97.03/98.50	93.93/95.69	75.80	68.06	51.95	-
SelectiveMAE	-	ViT-B	96.78/98.12	93.35/94.58	75.70	67.78	53.05	<b>79.50</b>
SelectiveMAE	-	ViT-L	<b>97.25/98.48</b>	<b>94.57/95.77</b>	<b>77.80</b>	<b>70.31</b>	<b>54.31</b>	79.46

available in our code. Evaluation is based on overall accuracy (OA). Table 6 presents the results, demonstrating SelectiveMAE’s competitive performance compared to other pre-training methods on both datasets. Notably, our method enjoys a significantly faster training speed, *e.g.*, over  $2\times$  faster than the MAE baseline. Besides, it outperforms RVSA and others when scaled to ViT-L. This demonstrates that, with our SelectiveMAE training method on the OpticalRS-4M dataset, the model can learn strong feature representations and scale efficiently.

**Horizontal & Oriented Object Detection.** We utilized the well-established DIOR dataset for horizontal object detection [87] and its improved variant DIOR-R for oriented object detection [88], both comprising RGB images. Following the methodologies of previous works [18, 37], we maintained consistent experimental setups, employing Faster-RCNN [89] and Oriented-RCNN [90] as detectors for each dataset. Detailed experimental configurations are available in the accompanying code. The results are summarized in Table 6. Our approach, utilizing a ViT-B backbone, demonstrates competitive or superior performance compared to other methods with a Swin-B backbone, such as RingMo [37]. When using the larger ViT-L backbone, SelectiveMAE shows enhanced performance across both detection datasets, underscoring the excellent scalability of our method.

**Semantic Segmentation.** We further evaluate the performance of the pre-trained model on pixel-level perception tasks, particularly semantic segmentation, using two well-known remote sensing datasets: LoveDA [51] and SpaceNetv1 [52]. Our implementation closely follows [18], utilizing UperNet [91] as the segmentation framework, with mean Intersection over Union (mIoU) as the evaluation metric. Table 6 demonstrates the clear superiority of SelectiveMAE over its competitors in pixel-level semantic segmentation. The selection and reconstruction strategies employed by SelectiveMAE focus on semantically rich patches, such as the boundaries between foreground objects and background stuff, leading to better representation learning for segmentation.

## 5 Conclusion

In this paper, we introduce a new pre-training pipeline for RS models, featuring the creation of a large-scale RS dataset and an efficient MIM approach. Built upon it, we first curated OpticalRS-4M, a large-scale optical remote sensing dataset for unsupervised learning. Unlike previous RS datasets, OpticalRS-4M offers a larger and more diverse image set with fine-grained details relevant to downstream tasks. Benchmarking representative MIM methods on OpticalRS-4M highlights its advantages in these tasks. Then, we present SelectiveMAE to reduce the computational overhead of MIM training on large-scale RS datasets. This efficient MIM method dynamically encodes and reconstructs tokens based on their semantic richness. SelectiveMAE significantly accelerates training, demonstrating that only 40% RS image patches are needed to train a comparable MIM model. Extensive experiments demonstrate that OpticalRS-4M significantly improves classification, detection, and segmentation performance, while SelectiveMAE achieves over  $2\times$  speedup, highlighting the effectiveness and scalability of our pipeline in developing RS foundational models.

## References

- [1] Nathalie Pettorelli, Henrike Schulte to Bühne, Ayesha Tulloch, Grégoire Dubois, Cate Macinnis-Ng, Ana M Queirós, David A Keith, Martin Wegmann, Franziska Schrodt, Marion Stellmes, et al. Satellite remote sensing of ecosystem functions: opportunities, challenges and way forward. *Remote Sensing in Ecology and Conservation*, 4(2):71–93, 2018.
- [2] Olalekan Mumin Bello and Yusuf Adedoyin Aina. Satellite remote sensing as a tool in disaster management and sustainable development: towards a synergistic approach. *Procedia-Social and Behavioral Sciences*, 120:365–373, 2014.
- [3] Liang Huang, Fengxiang Wang, Yalun Zhang, and Qingxia Xu. Fine-grained ship classification by combining cnn and swin transformer. *Remote Sensing*, 14(13):3087, 2022.
- [4] Fengxiang Wang, Deying Yu, Liang Huang, Yalun Zhang, Yongbing Chen, and Zhiguo Wang. Fine-grained ship image classification and detection based on a vision transformer and multi-grain feature vector fpn model. *Geo-spatial Information Science*, pages 1–22, 2024.
- [5] Tongdi He and Shengxin Wang. Multi-spectral remote sensing land-cover classification based on deep learning methods. *The Journal of Supercomputing*, 77(3):2829–2843, 2021.
- [6] Gong Cheng, Xingxing Xie, Junwei Han, Lei Guo, and Gui-Song Xia. Remote sensing image scene classification meets deep learning: Challenges, methods, benchmarks, and opportunities. *IEEE Journal of Selected Topics in Applied Earth Observations and Remote Sensing*, 13:3735–3756, 2020.
- [7] Wentong Li, Yijie Chen, Kaixuan Hu, and Jianke Zhu. Oriented reppoints for aerial object detection. In *Proceedings of the IEEE/CVF Conference on Computer Vision and Pattern Recognition (CVPR)*, pages 1829–1838, June 2022.
- [8] Curtis E Woodcock, Thomas R Loveland, Martin Herold, and Marvin E Bauer. Transitioning from change detection to monitoring with remote sensing: A paradigm shift. *Remote Sensing of Environment*, 238:111558, 2020.
- [9] Xiaohui Yuan, Jianfang Shi, and Lichuan Gu. A review of deep learning methods for semantic segmentation of remote sensing imagery. *Expert Systems with Applications*, 169:114417, 2021.
- [10] Kaiming He, Xinlei Chen, Saining Xie, Yanghao Li, Piotr Dollár, and Ross Girshick. Masked Autoencoders Are Scalable Vision Learners. In *CVPR*, 2022.
- [11] Zhenda Xie, Zheng Zhang, Yue Cao, Yutong Lin, Jianmin Bao, Zhuliang Yao, Qi Dai, and Han Hu. Simmim: A simple framework for masked image modeling. In *Proceedings of the IEEE/CVF conference on computer vision and pattern recognition*, pages 9653–9663, 2022.
- [12] Yufei Xu, Jing Zhang, Qiming Zhang, and Dacheng Tao. Vitpose: Simple vision transformer baselines for human pose estimation. *Advances in Neural Information Processing Systems*, 35:38571–38584, 2022.
- [13] Qiming Zhang, Yufei Xu, Jing Zhang, and Dacheng Tao. Vitaev2: Vision transformer advanced by exploring inductive bias for image recognition and beyond. *International Journal of Computer Vision*, 131(5):1141–1162, 2023.
- [14] Yufei Xu, Jing Zhang, Qiming Zhang, and Dacheng Tao. Vitpose++: Vision transformer for generic body pose estimation. *IEEE Transactions on Pattern Analysis and Machine Intelligence*, 2023.
- [15] Qiming Zhang, Jing Zhang, Yufei Xu, and Dacheng Tao. Vision transformer with quadrangle attention. *IEEE Transactions on Pattern Analysis and Machine Intelligence*, 2024.
- [16] Fengxiang Wang, Wanrong Huang, Shaowu Yang, Qi Fan, and Long Lan. Learning to learn better visual prompts. In *Proceedings of the AAAI Conference on Artificial Intelligence*, volume 38, pages 5354–5363, 2024.

- [17] Jingyi Wang, Xiaobo Xia, Long Lan, Xinghao Wu, Jun Yu, Wenjing Yang, Bo Han, and Tongliang Liu. Tackling noisy labels with network parameter additive decomposition. *IEEE Transactions on Pattern Analysis and Machine Intelligence*, 2024.
- [18] Di Wang, Qiming Zhang, Yufei Xu, Jing Zhang, Bo Du, Dacheng Tao, and Liangpei Zhang. Advancing plain vision transformer toward remote sensing foundation model. *IEEE Transactions on Geoscience and Remote Sensing*, 61:1–15, 2023.
- [19] Tal Ridnik, Emanuel Ben-Baruch, Asaf Noy, and Lihi Zelnik-Manor. Imagenet-21k pretraining for the masses. *arXiv preprint arXiv:2104.10972*, 2021.
- [20] Yang Long, Gui-Song Xia, Shengyang Li, Wen Yang, Michael Ying Yang, Xiao Xiang Zhu, Liangpei Zhang, and Deren Li. On creating benchmark dataset for aerial image interpretation: Reviews, guidances and million-aid. *IEEE Journal of Selected Topics in Applied Earth Observations and Remote Sensing*, 14:4205–4230, 2021.
- [21] Utkarsh Mall, Bharath Hariharan, and Kavita Bala. Change-aware sampling and contrastive learning for satellite images. In *Proceedings of the IEEE/CVF Conference on Computer Vision and Pattern Recognition*, pages 5261–5270, 2023.
- [22] Oscar Mañas, Alexandre Lacoste, Xavier Giró-i Nieto, David Vazquez, and Pau Rodríguez. Seasonal Contrast: Unsupervised Pre-Training From Uncurated Remote Sensing Data. In *ICCV*, 2021.
- [23] Gencer Sumbul, Arne de Wall, Tristan Kreuziger, Filipe Marcelino, Hugo Costa, Pedro Benevides, Mário Caetano, Begüm Demir, and Volker Markl. BigEarthNet-MM: A Large-Scale, Multimodal, Multilabel Benchmark Archive for Remote Sensing Image Classification and Retrieval [Software and Data Sets]. *IEEE Geoscience and Remote Sensing Magazine*, 2021.
- [24] Kumar Ayush, Burak Uzket, Chenlin Meng, Kumar Tanmay, Marshall Burke, David Lobell, and Stefano Ermon. Geography-Aware Self-Supervised Learning. In *ICCV*, 2021.
- [25] Matías Mendieta, Boran Han, Xingjian Shi, Yi Zhu, and Chen Chen. Towards geospatial foundation models via continual pretraining. In *Proceedings of the IEEE/CVF International Conference on Computer Vision*, pages 16806–16816, 2023.
- [26] Ziyue Huang, Mingming Zhang, Yuan Gong, Qingjie Liu, and Yunhong Wang. Generic knowledge boosted pre-training for remote sensing images. *IEEE Transactions on Geoscience and Remote Sensing*, 2024.
- [27] Di Wang, Jing Zhang, Bo Du, Minqiang Xu, Lin Liu, Dacheng Tao, and Liangpei Zhang. SAMRS: Scaling-up remote sensing segmentation dataset with segment anything model. *Advances in Neural Information Processing Systems*, 36, 2024.
- [28] Chao Tao, Ji Qi, Guo Zhang, Qing Zhu, Weipeng Lu, and Haifeng Li. Tov: The original vision model for optical remote sensing image understanding via self-supervised learning. *IEEE Journal of Selected Topics in Applied Earth Observations and Remote Sensing*, 2023.
- [29] Keumgang Cha, Junghoon Seo, and Taekyung Lee. A billion-scale foundation model for remote sensing images. *arXiv preprint arXiv:2304.05215*, 2023.
- [30] Yezhen Cong, Samar Khanna, Chenlin Meng, Patrick Liu, Erik Rozi, Yutong He, Marshall Burke, David Lobell, and Stefano Ermon. Satmae: Pre-training transformers for temporal and multi-spectral satellite imagery. *Advances in Neural Information Processing Systems*, 35:197–211, 2022.
- [31] Fanglong Yao, Wanxuan Lu, Heming Yang, Liangyu Xu, Chenglong Liu, Leiye Hu, Hongfeng Yu, Nayu Liu, Chubo Deng, Deke Tang, et al. Ringmo-sense: Remote sensing foundation model for spatiotemporal prediction via spatiotemporal evolution disentangling. *IEEE Transactions on Geoscience and Remote Sensing*, 2023.
- [32] Wenyan Li, Keyan Chen, and Zhenwei Shi. Geographical supervision correction for remote sensing representation learning. *IEEE Transactions on Geoscience and Remote Sensing*, 60:1–20, 2022.

- [33] Colorado J. Reed, Ritwik Gupta, Shufan Li, Sarah Brockman, Christopher Funk, Brian Clipp, Kurt Keutzer, Salvatore Candido, Matt Uyttendaele, and Trevor Darrell. Scale-MAE: A Scale-Aware Masked Autoencoder for Multiscale Geospatial Representation Learning. *CoRR*, abs/2212.14532, 2023.
- [34] Di Wang, Jing Zhang, Minqiang Xu, Lin Liu, Dongsheng Wang, Erzhong Gao, Chengxi Han, Haonan Guo, Bo Du, Dacheng Tao, and Liangpei Zhang. Mtp: Advancing remote sensing foundation model via multi-task pretraining. *IEEE Journal of Selected Topics in Applied Earth Observations and Remote Sensing*, pages 1–24, 2024.
- [35] Maofeng Tang, Andrei Liviu Cozma, Konstantinos Georgiou, and Hairong Qi. Cross-scale mae: A tale of multiscale exploitation in remote sensing. In *Thirty-seventh Conference on Neural Information Processing Systems*, 2023.
- [36] Mubashir Noman, Muzammal Naseer, Hisham Cholakkal, Rao Muhammad Anwar, Salman Khan, and Fahad Shahbaz Khan. Rethinking transformers pre-training for multi-spectral satellite imagery. In *CVPR*, 2024.
- [37] Xian Sun, Peijin Wang, Wanxuan Lu, Zicong Zhu, Xiaonan Lu, Qibin He, Junxi Li, Xuee Rong, Zhujun Yang, Hao Chang, et al. Ringmo: A remote sensing foundation model with masked image modeling. *IEEE Transactions on Geoscience and Remote Sensing*, 2022.
- [38] Dilxat Muhtar, Xueliang Zhang, Pengfeng Xiao, Zhenshi Li, and Feng Gu. Cmid: A unified self-supervised learning framework for remote sensing image understanding. *IEEE Transactions on Geoscience and Remote Sensing*, 61:1–17, 2023.
- [39] Alexey Dosovitskiy, Lucas Beyer, Alexander Kolesnikov, Dirk Weissenborn, Xiaohua Zhai, Thomas Unterthiner, Mostafa Dehghani, Matthias Minderer, Georg Heigold, Sylvain Gelly, Jakob Uszkoreit, and Neil Houlsby. An Image is Worth 16x16 Words: Transformers for Image Recognition at Scale. In *ICLR*, 2021.
- [40] Agrim Gupta, Jiajun Wu, Jia Deng, and Fei-Fei Li. Siamese masked autoencoders. *Advances in Neural Information Processing Systems*, 36, 2024.
- [41] Haoqing Wang, Yehui Tang, Yunhe Wang, Jianyuan Guo, Zhi-Hong Deng, and Kai Han. Masked image modeling with local multi-scale reconstruction. In *Proceedings of the IEEE/CVF Conference on Computer Vision and Pattern Recognition*, pages 2122–2131, 2023.
- [42] Jin Li, Yaoming Wang, Xiaopeng Zhang, Yabo Chen, Dongsheng Jiang, Wenrui Dai, Chenglin Li, Hongkai Xiong, and Qi Tian. Progressively compressed auto-encoder for self-supervised representation learning. In *The Eleventh International Conference on Learning Representations*, 2022.
- [43] Jun Chen, Ming Hu, Boyang Li, and Mohamed Elhoseiny. Efficient self-supervised vision pretraining with local masked reconstruction. *arXiv preprint arXiv:2206.00790*, 2022.
- [44] Jianyuan Guo, Kai Han, Han Wu, Yehui Tang, Yunhe Wang, and Chang Xu. Fastmim: Expediting masked image modeling pre-training for vision. *arXiv preprint arXiv:2212.06593*, 2022.
- [45] Letian Fu, Long Lian, Renhao Wang, Baifeng Shi, Xudong Wang, Adam Yala, Trevor Darrell, Alexei A Efros, and Ken Goldberg. Rethinking patch dependence for masked autoencoders. *arXiv preprint arXiv:2401.14391*, 2024.
- [46] Ben G Weinstein, Sergio Marconi, Stephanie A Bohlman, Alina Zare, Aditya Singh, Sarah J Graves, and Ethan P White. A remote sensing derived data set of 100 million individual tree crowns for the national ecological observatory network. *Elife*, 10:e62922, 2021.
- [47] Gordon Christie, Neil Fendley, James Wilson, and Ryan Mukherjee. Functional map of the world. In *Proceedings of the IEEE Conference on Computer Vision and Pattern Recognition*, pages 6172–6180, 2018.

- [48] Jan Gasienica-Jozkowy, Mateusz Knapik, and Bogusław Cyganek. An ensemble deep learning method with optimized weights for drone-based water rescue and surveillance. *Integrated Computer-Aided Engineering*, 28(3):221–235, 2021.
- [49] Long Lan, Fengxiang Wang, Shuyan Li, Xiangtao Zheng, Zengmao Wang, and Xinwang Liu. Efficient prompt tuning of large vision-language model for fine-grained ship classification. *arXiv preprint arXiv:2403.08271*, 2024.
- [50] Gaetan Bahl, Mehdi Bahri, and Florent Lafarge. Single-shot end-to-end road graph extraction. In *Proceedings of the IEEE/CVF Conference on Computer Vision and Pattern Recognition*, pages 1403–1412, 2022.
- [51] Junjue Wang, Zhuo Zheng, Ailong Ma, Xiaoyan Lu, and Yanfei Zhong. LoveDA: A remote sensing land-cover dataset for domain adaptive semantic segmentation. In *NeurIPS Track on Datasets and Benchmarks*, volume 1, 2021.
- [52] Adam Van Etten, Dave Lindenbaum, and Todd M Bacastow. Spacenet: A remote sensing dataset and challenge series. *arXiv preprint arXiv:1807.01232*, 2018.
- [53] Michael Schmitt, Lloyd Haydn Hughes, Chunping Qiu, and Xiao Xiang Zhu. Sen12ms—a curated dataset of georeferenced multi-spectral sentinel-1/2 imagery for deep learning and data fusion. *arXiv preprint arXiv:1906.07789*, 2019.
- [54] Yi Wang, Nassim Ait Ali Braham, Zhitong Xiong, Chenying Liu, Conrad M Albrecht, and Xiao Xiang Zhu. Ssl4eo-s12: A large-scale multimodal, multitemporal dataset for self-supervised learning in earth observation [software and data sets]. *IEEE Geoscience and Remote Sensing Magazine*, 11(3):98–106, 2023.
- [55] Adam Stewart, Nils Lehmann, Isaac Corley, Yi Wang, Yi-Chia Chang, Nassim Ait Ait Ali Braham, Shradha Sehgal, Caleb Robinson, and Arindam Banerjee. Ssl4eo-l: Datasets and foundation models for landsat imagery. *Advances in Neural Information Processing Systems*, 36, 2024.
- [56] Favyen Bastani, Piper Wolters, Ritwik Gupta, Joe Ferdinando, and Aniruddha Kembhavi. Satlaspretrain: A large-scale dataset for remote sensing image understanding. In *Proceedings of the IEEE/CVF International Conference on Computer Vision*, pages 16772–16782, 2023.
- [57] Zhecheng Wang, Rajanie Prabha, Tianyuan Huang, Jiajun Wu, and Ram Rajagopal. Skyscript: A large and semantically diverse vision-language dataset for remote sensing. *Proceedings of the AAAI Conference on Artificial Intelligence*, 38(6):5805–5813, Mar. 2024.
- [58] Zilun Zhang, Tiancheng Zhao, Yulong Guo, and Jianwei Yin. Rs5m: A large scale vision-language dataset for remote sensing vision-language foundation model. *arXiv preprint arXiv:2306.11300*, 2023.
- [59] Tom Brown, Benjamin Mann, Nick Ryder, Melanie Subbiah, Jared D Kaplan, Prafulla Dhariwal, Arvind Neelakantan, Pranav Shyam, Girish Sastry, Amanda Askell, et al. Language models are few-shot learners. *Advances in neural information processing systems*, 33:1877–1901, 2020.
- [60] Mark Chen, Alec Radford, Rewon Child, Jeffrey Wu, Heewoo Jun, David Luan, and Ilya Sutskever. Generative pretraining from pixels. In *International conference on machine learning*, pages 1691–1703. PMLR, 2020.
- [61] Xiao Teng, Long Lan, Jing Zhao, Xueqiong Li, and Yuhua Tang. Highly efficient active learning with tracklet-aware co-cooperative annotators for person re-identification. *IEEE Transactions on Neural Networks and Learning Systems*, 2023.
- [62] Long Lan, Xiao Teng, Jing Zhang, Xiang Zhang, and Dacheng Tao. Learning to purification for unsupervised person re-identification. *IEEE Transactions on Image Processing*, 2023.
- [63] Kaiming He, Xinlei Chen, Saining Xie, Yanghao Li, Piotr Dollár, and Ross Girshick. Masked autoencoders are scalable vision learners. In *Proceedings of the IEEE/CVF conference on computer vision and pattern recognition*, pages 16000–16009, 2022.

- [64] Hangbo Bao, Li Dong, Songhao Piao, and Furu Wei. Beit: Bert pre-training of image transformers. In *International Conference on Learning Representations*, 2021.
- [65] Chen Wei, Haoqi Fan, Saining Xie, Chao-Yuan Wu, Alan Yuille, and Christoph Feichtenhofer. Masked feature prediction for self-supervised visual pre-training. In *Proceedings of the IEEE/CVF Conference on Computer Vision and Pattern Recognition*, pages 14668–14678, 2022.
- [66] Jinghao Zhou, Chen Wei, Huiyu Wang, Wei Shen, Cihang Xie, Alan Yuille, and Tao Kong. Image bert pre-training with online tokenizer. In *International Conference on Learning Representations*, 2021.
- [67] Hao Liu, Xinghua Jiang, Xin Li, Antai Guo, Yiqing Hu, Deqiang Jiang, and Bo Ren. The devil is in the frequency: Geminated gestalt autoencoder for self-supervised visual pre-training. In *Proceedings of the AAAI Conference on Artificial Intelligence*, volume 37, pages 1649–1656, 2023.
- [68] Yuge Shi, N Siddharth, Philip Torr, and Adam R Kosiorek. Adversarial masking for self-supervised learning. In *International Conference on Machine Learning*, pages 20026–20040. PMLR, 2022.
- [69] Gang Li, Heliang Zheng, Daqing Liu, Chaoyue Wang, Bing Su, and Changwen Zheng. Semmae: Semantic-guided masking for learning masked autoencoders. *Advances in Neural Information Processing Systems*, 35:14290–14302, 2022.
- [70] Shubham Tulsiani and Abhinav Gupta. Pixeltransformer: Sample conditioned signal generation. In *International Conference on Machine Learning*, pages 10455–10464. PMLR, 2021.
- [71] Chen Wei, Karttikeya Mangalam, Po-Yao Huang, Yanghao Li, Haoqi Fan, Hu Xu, Huiyu Wang, Cihang Xie, Alan Yuille, and Christoph Feichtenhofer. Diffusion models as masked autoencoders. In *Proceedings of the IEEE/CVF International Conference on Computer Vision*, pages 16284–16294, 2023.
- [72] Zhaowen Li, Zhiyang Chen, Fan Yang, Wei Li, Yousong Zhu, Chaoyang Zhao, Rui Deng, Liwei Wu, Rui Zhao, Ming Tang, et al. Mst: Masked self-supervised transformer for visual representation. *Advances in Neural Information Processing Systems*, 34:13165–13176, 2021.
- [73] Ioannis Kakogeorgiou, Spyros Gidaris, Bill Psomas, Yannis Avrithis, Andrei Bursuc, Konstantinos Karantzas, and Nikos Komodakis. What to hide from your students: Attention-guided masked image modeling. In *European Conference on Computer Vision*, pages 300–318. Springer, 2022.
- [74] Di Wang, Jing Zhang, Bo Du, Gui-Song Xia, and Dacheng Tao. An empirical study of remote sensing pretraining. *IEEE Transactions on Geoscience and Remote Sensing*, 61:1–20, 2023.
- [75] Xinye Wanyan, Sachith Seneviratne, Shuchang Shen, and Michael Kirley. Dino-mc: Self-supervised contrastive learning for remote sensing imagery with multi-sized local crops. *arXiv preprint arXiv:2303.06670*, 2023.
- [76] Jeremy Irvin, Lucas Tao, Joanne Zhou, Yuntao Ma, Langston Nashold, Benjamin Liu, and Andrew Y Ng. Usat: A unified self-supervised encoder for multi-sensor satellite imagery. *arXiv preprint arXiv:2312.02199*, 2023.
- [77] Xin Guo, Jiangwei Lao, Bo Dang, Yingying Zhang, Lei Yu, Lixiang Ru, Liheng Zhong, Ziyuan Huang, Kang Wu, Dingxiang Hu, et al. Skysense: A multi-modal remote sensing foundation model towards universal interpretation for earth observation imagery. *arXiv preprint arXiv:2312.10115*, 2023.
- [78] Boran Han, Shuai Zhang, Xingjian Shi, and Markus Reichstein. Bridging remote sensors with multisensor geospatial foundation models. *arXiv preprint arXiv:2404.01260*, 2024.
- [79] Nikolaos Ioannis Bountos, Arthur Ouaknine, and David Rolnick. Fomo-bench: a multi-modal, multi-scale and multi-task forest monitoring benchmark for remote sensing foundation models. *arXiv preprint arXiv:2312.10114*, 2023.

- [80] Danfeng Hong, Bing Zhang, Xuyang Li, Yuxuan Li, Chenyu Li, Jing Yao, Pedram Ghamisi, Naoto Yokoya, Hao Li, Xiuping Jia, Antonio Plaza, et al. Spectralgpt: Spectral remote sensing foundation model. *IEEE Transactions on Pattern Analysis and Machine Intelligence*, 2024. DOI:10.1109/TPAMI.2024.3362475.
- [81] Chuan Qin, Meihui Sun, and Chin-Chen Chang. Perceptual hashing for color images based on hybrid extraction of structural features. *Signal processing*, 142:194–205, 2018.
- [82] Xin Wang, Yudong Chen, and Wenwu Zhu. A survey on curriculum learning. *IEEE transactions on pattern analysis and machine intelligence*, 44(9):4555–4576, 2021.
- [83] Yoshua Bengio, Jérôme Louradour, Ronan Collobert, and Jason Weston. Curriculum learning. In *Proceedings of the 26th annual international conference on machine learning*, pages 41–48, 2009.
- [84] Guy Hachohen and Daphna Weinshall. On the power of curriculum learning in training deep networks. In *International conference on machine learning*, pages 2535–2544. PMLR, 2019.
- [85] Gui-Song Xia, Jingwen Hu, Fan Hu, Baoguang Shi, Xiang Bai, Yanfei Zhong, Liangpei Zhang, and Xiaoqiang Lu. Aid: A benchmark data set for performance evaluation of aerial scene classification. *IEEE Transactions on Geoscience and Remote Sensing*, 55(7):3965–3981, 2017.
- [86] Gong Cheng, Junwei Han, and Xiaoqiang Lu. Remote sensing image scene classification: Benchmark and state of the art. *Proceedings of the IEEE*, 105(10):1865–1883, 2017.
- [87] Ke Li, Gang Wan, Gong Cheng, Liqiu Meng, and Junwei Han. Object detection in optical remote sensing images: A survey and a new benchmark. *ISPRS journal of photogrammetry and remote sensing*, 159:296–307, 2020.
- [88] Gong Cheng, Jiabao Wang, Ke Li, Xingxing Xie, Chunbo Lang, Yanqing Yao, and Junwei Han. Anchor-free oriented proposal generator for object detection. *IEEE Transactions on Geoscience and Remote Sensing*, 60:1–11, 2022.
- [89] Shaoqing Ren, Kaiming He, Ross Girshick, and Jian Sun. Faster r-cnn: Towards real-time object detection with region proposal networks. *IEEE Transactions on Pattern Analysis and Machine Intelligence*, 39(6):1137–1149, 2017.
- [90] Xingxing Xie, Gong Cheng, Jiabao Wang, Xiwen Yao, and Junwei Han. Oriented r-cnn for object detection. In *Proceedings of the IEEE/CVF International Conference on Computer Vision (ICCV)*, pages 3520–3529, October 2021.
- [91] Tete Xiao, Yingcheng Liu, Bolei Zhou, Yuning Jiang, and Jian Sun. Unified perceptual parsing for scene understanding. In *Proceedings of the European conference on computer vision (ECCV)*, pages 418–434, 2018.